



## Possible antiferroelectric-to-ferroelectric transition and metallic antiferroelectricity caused by charge doping in $\text{PbZrO}_3$

Huaxiang Fu *Department of Physics, University of Arkansas, Fayetteville, Arkansas 72701, USA* (Received 24 June 2020; revised 7 October 2020; accepted 12 October 2020; published 26 October 2020)

Using linear-response density functional calculations we study how the soft modes at both the zone center and the zone boundary are influenced by charge doping in cubic  $\text{PbZrO}_3$ . We find (i) upon the electron doping of  $n = -0.5$  per unit cell, the soft-mode frequency at zone-center  $\Gamma$  becomes considerably lower than that at the zone-boundary  $R$ , showing that electron doping may turn antiferroelectric  $\text{PbZrO}_3$  into ferroelectric. (ii) On the other hand, when the hole is doped into  $\text{PbZrO}_3$ , the soft mode at  $R$  or  $M$  remains to be the lowest in frequency, and therefore antiferroelectric instability is robust and persists after hole doping. Since hole doping makes  $\text{PbZrO}_3$  metallic, the coexistence of metallicity and antiferroelectricity demonstrates the feasibility of metallic antiferroelectricity. (iii) Electron doping and hole doping are revealed to impact the atom-atom interaction very differently. The origin responsible for these charge-doping phenomena is provided.

DOI: [10.1103/PhysRevB.102.134118](https://doi.org/10.1103/PhysRevB.102.134118)

### I. INTRODUCTION

Antiferroelectrics (AFE) are of significant importance both fundamentally and technologically [1,2]. Fundamentally, it is a long-standing challenge to formulate theoretically the antiferroelectric phase transitions [1,3,4]. Unlike ferroelectric phase transition, it is nontrivial to define an order parameter in AFE phase transformations. Furthermore, AFE materials exhibit multiple structural instabilities at different regions of the phonon Brillouin zone [5–7], and the intriguing competition among different instabilities often leads to unexpected structure phases and new phenomena [5–10]. Technologically, AFEs could drastically enhance the energy storage [11,12] by possessing double hysteresis and high saturated polarization under external electric fields [13]. Also, antiferroelectric  $\text{PbZrO}_3$  can be alloyed with ferroelectric  $\text{PbTiO}_3$  to form the morphotropic phase boundary between the rhombohedral phase and the tetragonal phase of  $\text{Pb}(\text{ZrTi})\text{O}_3$  [14,15], which is critical in producing the ultrahigh electromechanical response caused by polarization rotation [16–18].

Recently, another and separate subject is attracting much attention in the field of ferroelectricity, that is, charge doping in ferroelectrics (FEs). Ferroelectricity is caused by the delicate balance of long-range (LR) and short-range (SR) interactions [19–21]. Charge doping profoundly reduces the LR interaction in FEs by effective charge screening, which may entirely eliminate the polar instability and ferroelectricity [22]. Metallicity and polar distortion thus mutually repel, and are not anticipated to coexist in the same material [23]. That explains why the coexistence of polar instability and metallicity, such as in polar metals proposed by Anderson and Blount [24], is an intriguing phenomenon. Polar metals were indeed discovered in experiments, where metallic  $\text{LiOsO}_3$  was shown to undergo a ferroelectriclike structural transformation when temperature is lowered [25]. Another common route to

generate polar metals is by charge doping in FEs [26,27]. While the origin of polar metals is still unsettled, previous studies have pointed to the possibilities of short-range interaction [26,28,29], the Jahn-Teller effect [27], the decoupling of the electron states near the Fermi level from ferroelectric displacements [30,31], the meta-screening effect [32], and the charge-induced strong mode-mode coupling [33].

Compared to charge doping in FEs, charge doping in AFEs is much less understood and potentially more interesting, since in AFEs there are strong competing structural instabilities at zone boundaries as well as at zone center [5–7], and the subject on how charge doping affects these multiple instabilities and their competitions is intriguing. Indeed, many questions of profound relevance remain to be answered regarding charge doping in AFEs:

(i) How does charge doping alter the antiferroelectricity? Will it drastically strengthen, or weaken, the AFE instability?

(ii) Is there any interesting possibility that charge doping may turn antiferroelectricity into ferroelectricity?

(iii) How can charge doping be used to tune the relative instability of soft modes at different parts of the Brillouin zone, and thus potentially control the structural phases?

(iv) How does the charge doping alter the atom-atom interaction in AFEs? Answers to these questions not only yield a better understanding of the charge-doping physics, but also provide insight on how to engineer AFE materials for better functionalities.

In this paper we perform first-principles linear response calculations to investigate how charge doping may alter soft modes and structural instabilities in (centrosymmetric) cubic  $\text{PbZrO}_3$ , which is an important and prototypical antiferroelectric material. Structural instabilities both at the zone center and at the zone boundary are examined. We find that doping electrons and doping holes in  $\text{PbZrO}_3$  have very different effects. Under hole doping,  $\text{PbZrO}_3$  remains to be

strongly AFE while being metallic, and thereby the system becomes a metallic antiferroelectric. On the other hand, electron doping weakens the antiferroelectricity and enhances the ferroelectricity. As a consequence, electron doping may cause an interesting phase transition by turning antiferroelectric PbZrO<sub>3</sub> into ferroelectric. We further unveil that charge doping could significantly change the atom-atom interaction in PbZrO<sub>3</sub>. These results show that there is rich and interesting physics to learn about charge doping in AFEs.

## II. THEORETICAL METHODS

The structural instability under charge doping is investigated theoretically by determining the properties of the soft modes throughout the phonon Brillouin zone in cubic PbZrO<sub>3</sub>. When a solid is in the unstable centrosymmetric structure phase, soft modes with imaginary frequencies occur. By comparing the soft modes at the zone center (which often lead to ferroelectricity) and at the zone boundary (which may lead to antiferroelectricity) in terms of their frequencies, one may infer which structural instability is likely to prevail [6]. Obviously soft modes alone may not fully determine the structure phase, since other factors such as strain-mode coupling and multimode interaction may play roles when the solid is relaxed according to the soft modes [5,7]. It is also worth pointing out that soft modes at the zone boundary do not always lead to antiferroelectricity; for instance, the soft modes at the zone boundary may lead to the rotation of oxygen octahedra rather than antiferroelectricity.

We use the density-functional perturbation theory (DFPT) to calculate the frequencies and phonon eigendisplacements of lattice vibration [34–36]. When atoms vibrate, the shifts of atoms induce a deformation potential  $\Delta V(\mathbf{r})$  of bare ions, which is treated as perturbation. The linear response of electron state  $\Delta\psi_i(\mathbf{r})$  is computed by solving the Sternheimer equation [34,35]

$$(H_{scf} - \varepsilon_i)|\Delta\psi_i\rangle = -(\Delta V_{scf} - \Delta\varepsilon_i)|\psi_i\rangle, \quad (1)$$

where  $H_{scf}$  is the Kohn-Sham Hamiltonian,  $\varepsilon_i$  is the eigenvalue of  $H_{scf}$ ,  $\Delta V_{scf}(\mathbf{r}) = \Delta V(\mathbf{r}) + e \int \frac{\Delta\rho(\mathbf{r}')}{|\mathbf{r}-\mathbf{r}'|} d\mathbf{r}' + \frac{dv_{sc}(\rho)}{d\rho}\bigg|_{\rho=\rho(\mathbf{r})} \Delta\rho(\mathbf{r})$  is the first-order correction to the  $V_{scf}(\mathbf{r})$  potential, and  $\Delta\varepsilon_i = \langle\psi_i|\Delta V_{scf}(\mathbf{r})|\psi_i\rangle$  is the first-order correction to eigenvalue  $\varepsilon_i$ .

We consider a five-atom cubic cell to study soft modes. An alternative approach is to use the centrosymmetric atom positions in orthorhombic *Pbam* structure of  $\sqrt{2} \times 2\sqrt{2} \times 2$  unit cell with 40 atoms [37]. For the centrosymmetric phase, two different approaches are equivalent due to the folding effect of phonon bands [38]. We would also like to point out that, by doping an electron or hole in a five-atom bulk cell, the system becomes metallic by construction. There is a possibility that charge doping might introduce defects, polarons, or charge density waves, which are not considered here since they require large supercells.

We add (or remove) a given amount of electron per five-atom unit cell, denoted as  $n$ , to PbZrO<sub>3</sub> in order to study the electron doping (or hole doping), where  $n$  is negative for electron doping and positive for hole doping.  $n$  is chosen to range from  $-0.5$  to  $+0.5$  per unit cell. To avoid the

diverging Coulomb energy in a charged system with periodicity, a compensating uniform charge jellium is added [39]. It should be pointed out that charge doping may alter the lattice constant and volume of cubic PbZrO<sub>3</sub>. For each charge-doping concentration  $n$ , we optimize the lattice constant by minimizing the total energy while constraining the system to be cubic.

We have also examined whether charge doping will alter the cubic shape of the five-atom cell by performing calculations to optimize the cell shape under a given  $n$ . More specifically, we start with an orthorhombic cell, and constrain atoms to be at centrosymmetric positions (since our purpose is to investigate the soft modes). Then we optimize the cell shape using the stress tensor. We find that, for  $n = -0.5$  and  $n = +0.5$ , the cell shape is relaxed to the cubic structure, which justifies to some extent the optimization of cell volume while constraining the cubic symmetry.

Technically the first-principles density functional theory (DFT) within the local-density approximation (LDA) is employed [40]. Computations are performed using Quantum Espresso [41,42]. Troullier-Martins pseudopotentials are used to mimic the effects of core electrons [43]. Details of pseudopotentials were described in Ref. [44]. The cutoff energy for the plane-wave expansion of single-particle Kohn-Sham orbitals is 80 Ry, which is tested to be sufficient. Monkhorst-Pack  $k$ -point mesh of  $6 \times 6 \times 6$  is used.

## III. RESULTS AND DISCUSSIONS

### A. Undoped PbZrO<sub>3</sub>

Since undoped PbZrO<sub>3</sub> is technologically important itself and is of considerable relevance to readers, we first describe our calculation results for undoped PbZrO<sub>3</sub>. For centrosymmetric (cubic) PbZrO<sub>3</sub> without doping (i.e.,  $n = 0$ ), our total-energy calculations yield a lattice constant of  $a = 4.10$  Å and a bulk modulus of  $B = 183$  GPa. These values agree well with the previous result of  $a = 4.12$  Å and  $B = 180$  GPa obtained from LAPW calculations [5]. Our theoretical lattice constant is slightly smaller than the experimental value (4.15 Å) [45]. The underestimation of our theoretical lattice constant may drive the phonon modes harder, and will slightly modify the charge carrier concentration that causes the AFE-to-FE phase transition to be described below. Our linear-response calculations of cubic PbZrO<sub>3</sub> produce a soft-mode frequency  $\omega_\Gamma = -138$  cm<sup>-1</sup> at the zone center  $\Gamma$  and  $\omega_R = -191$  cm<sup>-1</sup> at the zone boundary  $R$ . Here the imaginary frequencies of soft modes are denoted as negative values throughout the paper. These frequencies are in accord with the values  $\omega_\Gamma \approx -140$  cm<sup>-1</sup> and  $\omega_R \approx -199$  cm<sup>-1</sup>, respectively [6]. Furthermore, in our calculations, the high frequency dielectric  $\varepsilon_\infty$  constant of undoped PbZrO<sub>3</sub> is 6.88 while the effective  $Z_{33}$  charges are 3.91, 5.92,  $-2.48$ ,  $-2.48$ , and  $-4.85$ , respectively, for Pb, Zr, O<sub>1</sub>, O<sub>2</sub>, and O<sub>3</sub>, where O<sub>3</sub> is directly beneath Zr along the  $c$  axis. These  $Z_{33}$  values agree well with the results in Ref. [46]. Therefore our calculations are rather reliable.

It worths pointing out that, after doped by electron or hole, PbZrO<sub>3</sub> then becomes metallic. In the modern theory of polarization [47,48], the rigorous definition of electric polarization

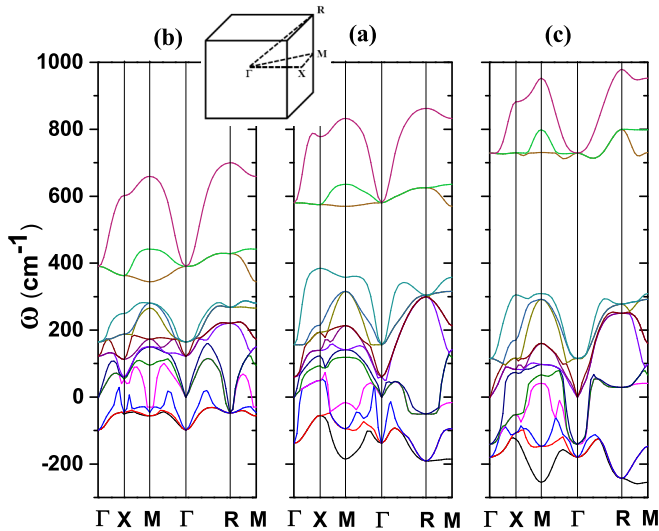


FIG. 1. Phonon dispersions of  $\text{PbZrO}_3$  under three different doping concentrations: (a)  $n = 0.0$  (undoped, the middle panel), (b)  $n = -0.5$  (electron doping, the left panel), and (c)  $n = +0.5$  (hole doping, the right panel). The cubic Brillouin zone and high-symmetry  $\Gamma$ ,  $X$ ,  $M$ , and  $R$  points are shown in the inset.

hinges on the adiabatic connection between ferroelectric state and paraelectric state via a path in which the system must remain to be insulating. The electric polarization, Born effective charges, and dielectric constant are thus ill-defined in metallic systems, so is the nonanalytical contribution in the theory of lattice dynamics [36]. Consequently, the longitudinal-optical (LO) phonon as well as the longitudinal-optical/transverse-optical (LO/TO) splitting are not well defined and cannot be calculated in metallic systems [49]. In order to make a valid comparison in phonon dispersion between undoped  $\text{PbZrO}_3$  (which is insulating) and doped  $\text{PbZrO}_3$  (which is metallic), we thus should not include the LO/TO splitting in phonon calculations for undoped  $\text{PbZrO}_3$ . We recognize that, when metallic heterostructures exhibit a strong anisotropy in Fermi surface, an interesting scheme was proposed to calculate the electric polarization [50].

The full-zone phonon dispersion of undoped  $\text{PbZrO}_3$ , obtained from the linear-response calculations, is given in Fig. 1(a). The plotted dispersion is along the path  $\Gamma \rightarrow X \rightarrow M \rightarrow \Gamma \rightarrow R \rightarrow M$ , where the reciprocal-space coordinates of the high-symmetry phonon wave vectors are (in units of  $\frac{2\pi}{a}$ )  $\Gamma(0, 0, 0)$ ,  $X(1/2, 0, 0)$ ,  $M(1/2, 1/2, 0)$ , and  $R(1/2, 1/2, 1/2)$ .

Figure 1(a) shows that (i) the soft mode at  $R$  has the lowest frequency ( $-191 \text{ cm}^{-1}$ ). The soft mode at zone-center  $\Gamma$  is significantly higher in frequency ( $-138 \text{ cm}^{-1}$ ). This is consistent with the fact that antiferroelectric instability prevails in undoped  $\text{PbZrO}_3$  [5,7]. (ii) The soft-mode frequency at  $M$  ( $-185 \text{ cm}^{-1}$ ) is comparable with that at  $R$ , and the dispersion of the lowest phonon band is notably flat along the line from  $R$  to  $M$  in Fig. 1(a). Furthermore, the lowest-frequency soft-mode dispersions are rather steep along the  $M \rightarrow X$ ,  $M \rightarrow \Gamma$ , and  $R \rightarrow \Gamma$  directions. (iii) The whole phonon dispersion in Fig. 1(a) can be roughly separated into two frequency regions: one is below  $400 \text{ cm}^{-1}$  (which will be denoted as “region I” and which includes many different phonon bands), and the

other is above  $400 \text{ cm}^{-1}$  (which will be denoted as “region II”).

## B. Electron doping

When a concentration of 0.5 electron per unit cell (i.e.,  $n = -0.5$ ) is doped into  $\text{PbZrO}_3$ , the phonon dispersion of electron-doped  $\text{PbZrO}_3$  is depicted in Fig. 1(b). Electron doping of  $n = -0.5$  per bulk cell will produce a charge concentration of  $7 \times 10^{21} e/\text{cm}^3$ . By contrasting the phonon dispersion of electron-doped  $\text{PbZrO}_3$  [Fig. 1(b)] with that of undoped  $\text{PbZrO}_3$  [Fig. 1(a)], we see several marked differences.

(i) First, Fig. 1(b) shows that, under electron doping of  $n = -0.5$ , the lowest-frequency soft mode in  $\text{PbZrO}_3$  is located at the zone-center  $\Gamma$ . This is in difference with Fig. 1(a) for undoped  $\text{PbZrO}_3$  where the lowest-frequency soft mode is at zone-boundary  $R$ .

(ii) Furthermore, the soft modes at  $R$  (or  $M$ ) in Fig. 1(b) are significantly higher in frequency than at  $\Gamma$ . The relatively large frequency difference between  $\Gamma$  and  $R$  signals that, under  $n = -0.5$ , the FE instability at  $\Gamma$  will be dominating in  $\text{PbZrO}_3$ , while the instability at  $R$  or  $M$  is only secondary. This is interesting and it reveals that, under  $n = -0.5$ ,  $\text{PbZrO}_3$  may become ferroelectric (not antiferroelectric). We thus predict a possibility that electron doping could cause a AFE-to-FE transition which turns antiferroelectric  $\text{PbZrO}_3$  into ferroelectric. Furthermore, we find that the dominance of instability at  $\Gamma$  can be further tuned by doping more electrons into  $\text{PbZrO}_3$ . In-plane strain may also turn  $\text{PbZrO}_3$  into ferroelectric [8].

(iii) Moreover, in Fig. 1(b), the frequencies of the lattice vibration in region I vary from  $-100$  to  $300 \text{ cm}^{-1}$  under  $n = -0.5$ , which amounts to a frequency range of about  $400 \text{ cm}^{-1}$ . This frequency range of region I is considerably reduced, as compared to the counterpart range of  $600 \text{ cm}^{-1}$  in Fig. 1(a) for undoped  $\text{PbZrO}_3$  (where frequencies vary from  $-200$  to  $400 \text{ cm}^{-1}$  in region I). Therefore, the electron doping alters both soft modes and nonsoft modes in a significant manner. It may worth mentioning that the frequency range of phonon dispersion is relevant since it is related to the strength of atom-atom interaction, similar to the fact that the bandwidth in electron band structure is correlated with the strength of chemical bonding.

Meanwhile, for phonons in region II [i.e., when frequencies are above  $300 \text{ cm}^{-1}$  in Fig. 1(b)], we observe that the frequencies in region II under  $n = -0.5$  are notably lower than those in Fig. 1(a) for undoped  $\text{PbZrO}_3$ . Namely, the frequencies in region II shift down upon electron doping.

We have also performed calculations for another electron-doping concentration at  $n = -0.25$ . The soft-mode frequencies at high-symmetry  $\Gamma$ ,  $X$ ,  $M$ , and  $R$  points for  $n = -0.25$ , in addition to  $n = -0.5$ , are given in Table I and are plotted in Fig. 2. Figure 2 (also Table I) shows that, at  $n = -0.25$ , the soft-mode frequencies  $\omega_\Gamma$ ,  $\omega_R$ , and  $\omega_M$  are comparable, and the competition and interplay of these soft modes will be strong. In addition, Fig. 2 reveals that, for electron doping (i.e., when  $n$  is negative), the soft-mode frequency at  $X$  does not change significantly, while frequencies at  $R$  and  $M$  increase drastically as  $n$  becomes more negative. As a consequence, at  $n = -0.5$ , the frequency ordering follows the sequence  $\omega_\Gamma < \omega_M < \omega_X < \omega_R$ , and the frequency at  $R$  or  $M$

TABLE I. Phonon frequencies of the lowest soft modes at  $\Gamma$ ,  $X$ ,  $M$ , and  $R$  in  $\text{PbZrO}_3$  under different doping concentration  $n$ . All frequencies are in units of  $\text{cm}^{-1}$ .

$n$	$\omega_\Gamma$	$\omega_X$	$\omega_M$	$\omega_R$
-0.50	-98	-51	-56	-48
-0.25	-111	-48	-116	-122
0.00	-138	-55	-185	-191
+0.25	-147	-47	-220	-223
+0.50	-180	-126	-255	-243

is only about half of that at  $\Gamma$ , as informed by Table I. The structural instability caused by  $\omega_\Gamma$  at the zone-center  $\Gamma$  is thus predominating.

To obtain the microscopic insight on which atoms are responsible for causing the ferroelectric instability under  $n = -0.5$ , we examine the phonon eigendisplacement of the soft mode at  $\Gamma$ . The phonon eigendisplacement  $|u_m^{i\alpha}\rangle$  at wave vector  $\mathbf{q}$  is related to the phonon eigenvector  $|\epsilon_m^{i\alpha}\rangle$  by  $|u_m^{i\alpha}\rangle = \frac{1}{\sqrt{M_i}}|\epsilon_m^{i\alpha}\rangle e^{i\mathbf{q}\cdot\mathbf{R}_i}$ , where  $M_i$  is the mass of atom  $i$ ,  $\alpha$  is the direction index,  $m$  is the mode index, and  $\mathbf{R}_i$  is a lattice vector. Since the three Cartesian directions are equivalent in cubic  $\text{PbZrO}_3$ , we will focus on the soft mode vibrating along the  $z$  axis. We find that, under  $n = -0.5$ , the normalized phonon eigendisplacement of the soft mode at  $\Gamma$  is  $(-0.18, 0.11, 0.61, 0.61, 0.46)_z$  in the sequence of Pb, Zr,  $O_1$ ,  $O_2$ , and  $O_3$  atoms, where subscript  $z$  means that the vibration is along the  $z$  axis, and atom  $O_3$  is located directly beneath the Zr atom along the  $z$  axis. The eigendisplacement of this soft mode at  $\Gamma$  is shown in Fig. 3. From the eigendisplacement in Fig. 3, we see that Pb and three O atoms are vibrating along opposite directions, showing that the soft mode is indeed ferroelectric. Meanwhile, Zr and O atoms vibrate along the same direction, and the Zr-O relative motion is thus not responsible for the ferroelectricity. Therefore, ferroelectricity in  $\text{PbZrO}_3$  under  $n = -0.5$  is mainly caused by the opposite motions of

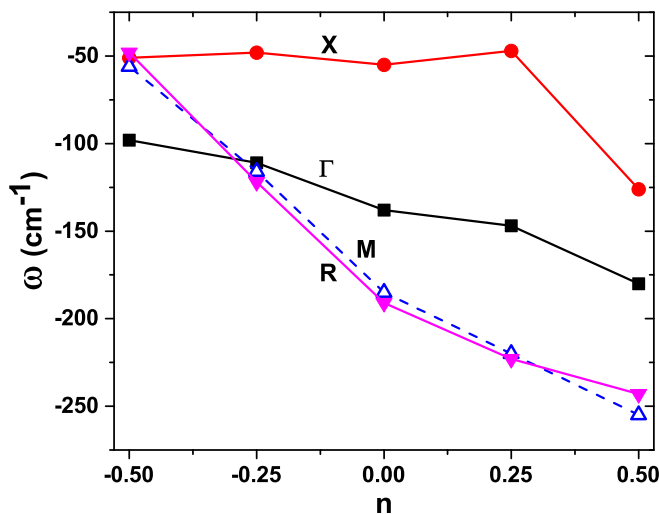


FIG. 2. Soft-mode frequencies at high-symmetry  $\Gamma$ ,  $X$ ,  $M$ , and  $R$  points as a function of charge-doping concentration  $n$ .  $n$  is negative for electron doping, and positive for hole doping.

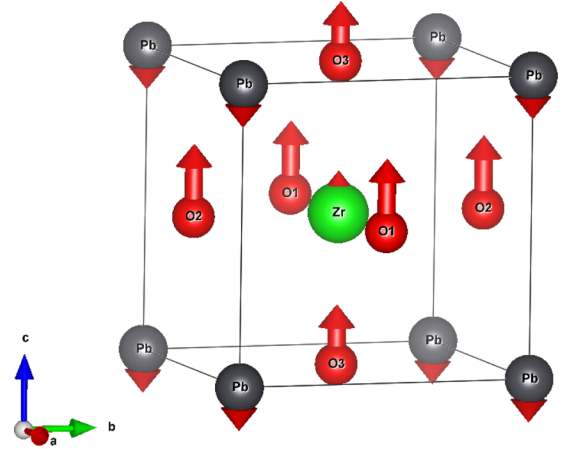


FIG. 3. The eigendisplacement of the soft mode at  $\Gamma$  in electron-doped  $\text{PbZrO}_3$  under  $n = -0.5$ .

Pb and O. The eigendisplacement further reveals that the soft mode at  $\Gamma$  in  $\text{PbZrO}_3$  under  $n = -0.5$  is a Last mode [51,52], which differs from  $\text{BaTiO}_3$  and  $\text{PbTiO}_3$  where the soft mode at  $\Gamma$  is a Slater mode [53] and ferroelectricity predominately comes from the opposite motion of Ti-O atoms.

To confirm that the AFE-to-FE transition will indeed occur in AFE  $\text{PbTiO}_3$  by electron doping, we have performed calculations by starting with the  $Pbam$  structure of antiferroelectric  $\text{PbZrO}_3$  with 40 atoms per supercell, doping the system with four electrons per supercell (which is equivalent to  $n = -0.5$  per bulk cell), and optimizing the atomic positions and cell shape. Then we use the optimized atomic positions and determine the relative atomic displacements with respect to those in the centrosymmetric cubic structure. We find that, after doping, the average displacements are 0.25, 0.02, and  $-0.15$  Å for Pb, Zr, and O atoms, respectively. In  $Pbam$  structure of AFE  $\text{PbZrO}_3$ , the supercell is a  $\sqrt{2} \times 2\sqrt{2} \times 2$  multiple of bulk cell. The above displacements are along the lattice vector of length  $2\sqrt{2}$ . The results show that (i) the average displacement of Pb atoms is large and nonzero, in contrast to the AFE structure where the average displacement of Pb atoms is zero, and (ii) the Pb atoms and the O atoms move along opposite directions, indicating that antiferroelectric  $\text{PbZrO}_3$  indeed becomes ferroelectric after electron doping.

The finding of the AFE-to-FE transition by electron doping in  $\text{PbZrO}_3$  is interesting. We now provide an explanation to understand the origin why electron doping causes the transition. We find that the reason is rather simple, and can be attributed to the lattice expansion triggered by electron doping. In Fig. 4 the lattice constant of cubic  $\text{PbZrO}_3$  as a function of doping concentration  $n$  is depicted, as determined by LDA optimization of total energy while constraining the cubic symmetry. Figure 4 reveals that, when electrons are doped into  $\text{PbZrO}_3$  (i.e., when  $n$  is negative),  $\text{PbZrO}_3$  expands and the lattice constant increases. Quantitatively, the lattice constant ( $a$ ) is calculated to be 4.100, 4.185, and 4.271 Å, respectively, for  $n = 0.0$ ,  $n = -0.25$ , and  $n = -0.50$ . The lattice constant is found to expand about 4% from  $n = 0$  to  $n = -0.5$ , which is rather substantial. It is known that larger cell volume tends to favor ferroelectricity while inhibiting the antiferroelectric distortion [54]. Furthermore, we have

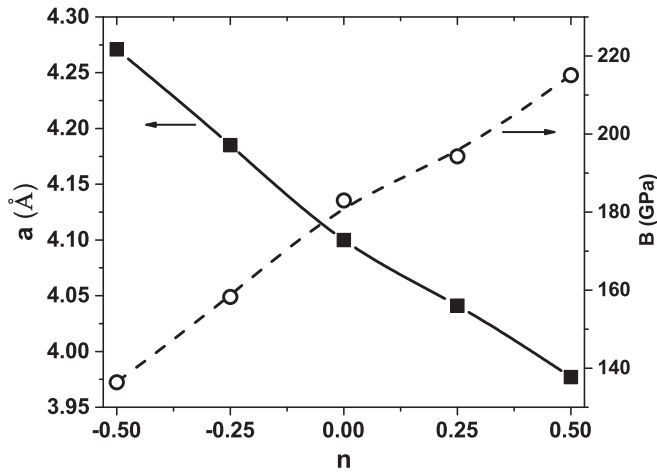


FIG. 4. LDA-optimized lattice constant  $a$  (solid squares, using the left vertical axis) and calculated bulk modulus  $B$  (empty circles, using the right vertical axis) of  $\text{PbZrO}_3$  as a function of charge-doping concentration  $n$ .

computed the phonon frequencies for  $n = -0.5$  while keeping the lattice constant to be the same as undoped  $\text{PbZrO}_3$ , and we find that the soft-mode frequencies  $\omega_\Gamma = -83 \text{ cm}^{-1}$  and  $\omega_R = -122 \text{ cm}^{-1}$ . In other words, if the lattice constant is artificially assumed to be unchanged, the AFE instability will remain to be predominating at  $n = -0.5$ . Therefore, the lattice expansion caused by electron doping is indeed responsible for turning antiferroelectric  $\text{PbZrO}_3$  into ferroelectric.

We next attempt to explain why electron doping may cause the frequency width of the phonon bands in region I to shrink, as observed in the above by comparing Fig. 1(b) with Fig. 1(a). For this purpose we recognize that the width of *phonon* bands is related to the atom-atom interaction, similar to the fact that the width of *electron* bands is related to electron-electron interaction. The width of the phonon bands in region I can be attributed to the decrease in interatomic interaction induced by electron doping. To confirm this, we calculate the bulk modulus of cubic  $\text{PbZrO}_3$  at its optimized lattice constant under different electron-doping concentrations, since bulk modulus is related to the overall strength of interatomic interaction. The bulk modulus of  $\text{PbZrO}_3$  is plotted as the empty circles in Fig. 4, showing that when  $n$  is negative, the bulk modulus declines substantially, from 183 GPa at  $n = 0$  to 136 GPa at  $n = -0.5$ . Therefore we find that the atom-atom interaction is indeed weakened by electron doping, which leads to the reduction of the frequency width of phonon bands in region I. Furthermore, for lattice vibration in region II [with frequencies larger than  $300 \text{ cm}^{-1}$  in Fig. 1(b)], these vibrations mainly originate from oxygen atoms, and the weakening of atom-atom interaction shall also lower the frequencies in region II, which is consistent with the calculation results in Fig. 1(b) as compared to Fig. 1(a).

Meanwhile we notice that the bandwidth of region II in Fig. 1(b) is slightly larger than in Fig. 1(a). One possible reason that the electron doping slightly enlarges the bandwidth of region II is the following. In region II the maximum phonon frequency  $\omega_{\max}$  is located at  $R$ , while the minimum frequency  $\omega_{\min}$  is located at  $M$  as shown in Fig. 1(b). The difference

between  $\omega_{\max}$  and  $\omega_{\min}$  determines the phonon bandwidth. By examining the phonon eigendisplacements, we find that, at  $\omega_{\max}$ , the phonon eigendisplacements are identical for  $n = 0$  and for  $n = -0.5$  due to symmetry. However, at  $\omega_{\min}$ , there is a weaker participation of Zr at  $n = -0.5$  (with a Zr amplitude of merely 0.018) than at  $n = 0$  (with a Zr amplitude of 0.102). The weaker participation of Zr at  $n = -0.5$  may be explained by the fact that part of the doping electrons occupy the Zr site, which causes an additional Coulomb repulsion between Zr and O atoms. The repulsion lowers the frequency  $\omega_{\min}$  in Fig. 1(b), and makes the phonon bandwidth larger in Fig. 1(b) than in Fig. 1(a).

### C. Hole doping

The phonon frequencies at high-symmetry  $\Gamma$ ,  $X$ ,  $M$ , and  $R$  points under two different hole doping concentrations (i.e.,  $n = +0.25$  and  $n = +0.5$ ) are given in Table I and are plotted in Fig. 2. First we need to point out that, under hole doping of  $n = +0.25$ ,  $\text{PbZrO}_3$  becomes metallic, since the Fermi level is located within the valence bands and there is mobile hole available. Table I shows that, under  $n = +0.25$ , the soft-mode frequency at  $R$  continues to be much lower than that at  $\Gamma$ , and the AFE instability continues to dominate, which is similar to the undoped case of  $n = 0$ . This similarity indicates that  $\text{PbZrO}_3$  remains to be antiferroelectric under hole doping. Our calculations thus reveal that metallicity and antiferroelectricity coexist in hole-doped  $\text{PbZrO}_3$ , or in other words,  $\text{PbZrO}_3$  under  $n = +0.25$  is a metallic antiferroelectric. It is likely that “metallic antiferroelectrics” may stimulate widespread interest in the future as “metallic ferroelectrics.”

Furthermore, several observations of important relevance can be made from Fig. 2 about hole doping. As hole-doping concentration increases from  $n = 0$  to  $n = +0.25$  and finally to  $n = +0.5$  in Fig. 2, we see (i) the soft-mode frequencies at  $R$ ,  $M$ , and  $\Gamma$  become more negative, and therefore we find that, as a general rule, *hole doping tends to enhance the structural instability* which includes the AFE instability at  $R$  as well as the FE instability at  $\Gamma$ . (ii) As  $n$  increases,  $\omega_M$  decreases slightly faster than  $\omega_R$ . As a result, at  $n = +0.5$ ,  $\omega_M$  becomes the lowest-frequency soft mode. (iii) In Fig. 2, the soft-mode ordering in terms of frequency, at  $n = +0.5$  of hole doping, is  $\omega_M < \omega_R < \omega_\Gamma < \omega_X$ , which is different from the ordering sequence  $\omega_\Gamma < \omega_M \approx \omega_X \approx \omega_R$  at  $n = -0.5$  of electron doping, showing that electron doping and hole doping produce very different effects.

It is no surprise that hole doping and electron doping should generate different effects. In  $\text{PbZrO}_3$ , the states at the low conduction bands are mainly contributed by Pb  $6s$  orbitals and Zr  $4d$  orbitals, while the states at the upper valence bands are mainly contributed by O  $2p$  orbitals [5]. Therefore, the doped electrons will largely stay at Pb and Zr sites, and in contrast, the doped holes will largely stay at the O sites, which in turn produces dissimilar impact on how atoms interact with the others.

The full-zone phonon dispersion of  $\text{PbZrO}_3$  under  $n = +0.5$  of hole doping is depicted in Fig. 1(c). Figure 1(c) shows that (i) the soft-mode frequency at  $R$  (also  $M$ ) is significantly lower than at other phonon wave vectors (such as at  $\Gamma$ ), confirming that the dominating structural instability is at  $R$  (and

$M$ ) under hole doping. (ii) Near zone-center  $\Gamma$ , several phonon bands anticross with each other, for instance, at frequencies of about  $-125$  and  $+150$   $\text{cm}^{-1}$ , leading to the characteristic waterfall-like phonon dispersion. The waterfall-like dispersion is caused by the mode-mode interaction [55,56]. (iii) By comparing Fig. 1(c) with Fig. 1(a), we see that hole doping increases significantly the frequencies in region II. Meanwhile, the width of phonon bands in region I is comparable in Fig. 1(c) and in Fig. 1(a).

We next examine how hole doping may alter the atom-atom interaction. We realize that there are two competing factors by which hole doping may influence the interaction among atoms. As the first competing factor, we find that hole doping shrinks the lattice constant. To illustrate this, we plot the optimized lattice constant under different amount of hole doping in Fig. 4. Figure 4 reveals that, when  $n$  is positive, lattice constant is reduced from  $a = 4.100$   $\text{\AA}$  at  $n = 0.0$  to  $a = 3.977$   $\text{\AA}$  at  $n = +0.50$ , telling us that the interatomic distances are considerably shortened by the hole doping. This will increase the short-range (SR) atom-atom interaction. As the second competing factor, we recognize that the hole doping may weaken the long-range (LR) interaction, since the doping allows mobile holes to be available in the valence bands, which will screen the LR Coulomb interaction. Competition between the enhanced SR interaction and the weakened LR interaction in hole-doped  $\text{PbZrO}_3$  breaks the delicate balance which previously exists in undoped  $\text{PbZrO}_3$ , and the new balance makes  $\text{PbZrO}_3$  under hole doping an interesting topic to tune the microscopic interaction in AFEs. To examine how the total (SR + LR) interaction is affected by hole doping, we compute the bulk modulus under different hole-doping concentration  $n$ , and the result is shown by the dash line in Fig. 4. Figure 4 reveals that, when  $n$  increases from 0 to  $+0.5$ , the bulk modulus increases from 183 to 215 GPa. Therefore, the total (SR + LR) interaction among atoms in  $\text{PbZrO}_3$  is significantly enhanced by hole doping.

We have also calculated the band structure of  $\text{PbZrO}_3$  under  $n = +0.5$ . The obtained band structure is shown in Fig. 5(c), in comparison with those of undoped system [Fig. 5(a)] and under electron doping of  $n = -0.5$  [Fig. 5(b)]. For undoped  $\text{PbZrO}_3$ , we find that it has a direct band gap of 2.37 eV at  $X$  [Fig. 5(a)], which is close to the band gap of 2.34 eV obtained from LAPW calculations [5]. Under electron doping of  $n = -0.5$ , the band gap of  $\text{PbZrO}_3$  becomes indirect between CBM at  $X$  and VBM at  $M$ , and the indirect gap is 2.14 eV [Fig. 5(b)]. Under hole doping of  $n = +0.5$ , the band gap is found to be 2.67 eV and is direct at  $X$  [Fig. 5(c)].

#### IV. CONCLUSIONS

We have performed first-principles linear response calculations to investigate the influence of electron doping and hole doping on the structural instability in technologically important antiferroelectric  $\text{PbZrO}_3$ . Our main findings are summarized as follows.

(i) Electron doping is shown to possibly turn antiferroelectric  $\text{PbZrO}_3$  into ferroelectric. The transition occurs around  $n = -0.25$ . The origin of this AFE-to-FE transition is simple, and it results from the lattice expansion induced by electron doping. The lattice expansion causes the soft mode at

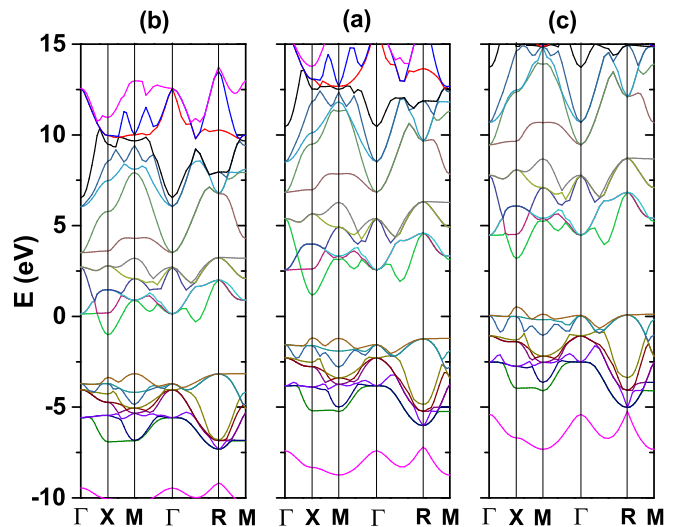


FIG. 5. Electronic band structures of  $\text{PbZrO}_3$  under three different doping concentrations: (a)  $n = 0.0$  (undoped, the middle panel), (b)  $n = -0.5$  (electron doping, the left panel), and (c)  $n = +0.5$  (hole doping, the right panel). The Fermi energy is set to be zero in each band structure.

the zone-center  $\Gamma$  to possess a significantly lower frequency than at zone boundary, which disfavors the antiferroelectric distortion at the zone boundary and favors the ferroelectricity at the zone center.

(ii) Microscopically, ferroelectricity in  $\text{PbZrO}_3$  under electron doping  $n = -0.5$  is associated with the opposite motions of Pb and O atoms. In contrast, the off-center displacements of Zr and O atoms are along the same direction. In other words, the soft mode which causes ferroelectricity in electron-doped  $\text{PbZrO}_3$  is the Last mode, which differs from  $\text{PbTiO}_3$  and  $\text{BaTiO}_3$  where the soft mode is largely the Slater mode.

(iii) We further reveal that, under *hole* doping, antiferroelectricity persists and is robust in  $\text{PbZrO}_3$ . Since hole doping makes the system metallic, our calculations thus suggest that it is possible for hole conductivity (metallicity) and antiferroelectricity to coexist in the same system. The interplay of metallicity and antiferroelectricity in  $\text{PbZrO}_3$  is an interesting new subject.

(iv) Electron doping is shown to weaken the atom-atom interaction as demonstrated by the significant reduction in the bulk modulus. In contrast, the hole doping increases the bulk modulus, and may cause a new balance in atomic interaction by enhancing the short-range interaction and weakening the long-range interaction.

These results show that there is rich and interesting physics to emerge by charge doping in antiferroelectrics. We hope that this study will stimulate more theoretical and experimental interest in this research field.

#### ACKNOWLEDGMENTS

This work was partially supported by the Office of Naval Research. Computations were performed on the computing facilities provided by the Arkansas High-Performance Computing Center, supported by NSF.

- [1] K. M. Rabe, *Functional Metal Oxides* (Wiley-VCH, Berlin, 2013).
- [2] M. E. Lines and A. M. Glass, *Principles and Applications of Ferroelectrics and Related Materials* (Clarendon, Oxford, 1979).
- [3] C. Kittel, *Phys. Rev.* **82**, 729 (1951).
- [4] P. Toledano and M. Guennou, *Phys. Rev. B* **94**, 014107 (2016).
- [5] D. J. Singh, *Phys. Rev. B* **52**, 12559 (1995).
- [6] P. Ghosez, E. Cockayne, U. V. Waghmare, and K. M. Rabe, *Phys. Rev. B* **60**, 836 (1999).
- [7] J. Iniguez, M. Stengel, S. Prosandeev, and L. Bellaiche, *Phys. Rev. B* **90**, 220103(R) (2014).
- [8] S. E. Reyes-Lillo and K. M. Rabe, *Phys. Rev. B* **88**, 180102(R) (2013).
- [9] A. K. Tagantsev, K. Vaideeswaran, S. B. Vakhrushev, A. V. Filimonov, R. G. Burkovsky, A. Shaganov, D. Andronikova, A. I. Rudskoy, A. Q. R. Baron, H. Uchiyama, D. Chernyshov, A. Bosak, Z. Ujma, K. Roleder, A. Majchrowski, J.-H. Ko, and N. Setter, *Nat. Commun.* **4**, 2229 (2013).
- [10] B. K. Mani, S. Lisenkov, and I. Ponomareva, *Phys. Rev. B* **91**, 134112 (2015).
- [11] X. Hao, *J. Adv. Dielectr.* **3**, 1330001 (2013).
- [12] X. Tan, C. Ma, J. Fredrick, S. Beckman, and K. G. Weber, *J. Am. Ceram. Soc.* **94**, 4091 (2011).
- [13] G. Shirane, E. Sawaguchi, and Y. Takagi, *Phys. Rev.* **84**, 476 (1951).
- [14] B. Noheda, D. E. Cox, G. Shirane, J. A. Gonzalo, L. E. Cross, and S.-E. Park, *Appl. Phys. Lett.* **74**, 2059 (1999).
- [15] B. Noheda, D. E. Cox, G. Shirane, S.-E. Park, L. E. Cross, and Z. Zhong, *Phys. Rev. Lett.* **86**, 3891 (2001).
- [16] S.-E. Park and T. R. Shrout, *J. Appl. Phys.* **82**, 1804 (1997).
- [17] A. Garcia and D. Vanderbilt, *Appl. Phys. Lett.* **72**, 2981 (1998).
- [18] H. Fu and R. E. Cohen, *Nature (London)* **403**, 281 (2000).
- [19] W. Cochran, *Adv. Phys.* **9**, 387 (1960).
- [20] R. E. Cohen, *Nature (London)* **358**, 136 (1992).
- [21] R. E. Cohen and H. Krakauer, *Phys. Rev. B* **42**, 6416 (1990).
- [22] L. D. Landau, L. P. Pitaevskii, and E. M. Lifshitz, *Electrodynamics of Continuous Media* (Elsevier Butterworth-Heinemann, Boston, 2004).
- [23] T. H. Kim, D. Puggioni, Y. Yuan, L. Xie, H. Zhou, N. Campbell, P. J. Ryan, Y. Choi, J.-W. Kim, J. R. Patzner, S. Ryu, J. P. Podkaminer, J. Irwin, Y. Ma, C. J. Fennie, M. S. Rzechowski, X. Q. Pan, V. Gopalan, J. M. Rondinelli, and C. B. Eom, *Nature (London)* **533**, 68 (2016).
- [24] P. W. Anderson and E. I. Blount, *Phys. Rev. Lett.* **14**, 217 (1965).
- [25] Y. Shi, Y. Guo, X. Wang, A. J. Princep, D. Khalyavin, P. Manuel, Y. Michiue, A. Sato, K. Tsuda, S. Yu, M. Arai, Y. Shirako, M. Akaogi, N. Wang, K. Yamaura, and A. T. Boothroy, *Nat. Mater.* **12**, 1024 (2013).
- [26] N. A. Benedek and T. Birol, *J. Mater. Chem. C* **4**, 4000 (2016).
- [27] X. He and K.-J. Jin, *Phys. Rev. B* **94**, 224107 (2016).
- [28] H. J. Xiang, *Phys. Rev. B* **90**, 094108 (2014).
- [29] G. Giovannetti and M. Capone, *Phys. Rev. B* **90**, 195113 (2014).
- [30] D. Puggioni, G. Giovannetti, M. Capone, and J. M. Rondinelli, *Phys. Rev. Lett.* **115**, 087202 (2015).
- [31] D. Puggioni and J. M. Rondinelli, *Nat. Commun.* **5**, 3432 (2014).
- [32] H. J. Zhao, A. Filippetti, C. Escorihuela-Sayalero, P. Delugas, E. Canadell, L. Bellaiche, V. Fiorentini, and J. Iniguez, *Phys. Rev. B* **97**, 054107 (2018).
- [33] Z. Yimer and H. Fu, *Phys. Rev. B* **101**, 174105 (2020).
- [34] S. Baroni, S. de Gironcoli, A. Dal Corso, and P. Giannozzi, *Rev. Mod. Phys.* **73**, 515 (2001).
- [35] S. Baroni, P. Giannozzi, and A. Testa, *Phys. Rev. Lett.* **58**, 1861 (1987).
- [36] X. Gonze, *Phys. Rev. A* **52**, 1096 (1995).
- [37] H. Fujishita, Y. Ishikawa, S. Tanaka, A. Ogawaguchi, and S. Katano, *J. Phys. Soc. Jpn.* **72**, 1426 (2003).
- [38] P. Yu and M. Cardona, *Fundamentals of Semiconductors* (Springer, Berlin, 2001).
- [39] Y. Yao and H. Fu, *Phys. Rev. B* **84**, 064112 (2011).
- [40] P. Hohenberg and W. Kohn, *Phys. Rev.* **136**, B864 (1964); W. Kohn and L. J. Sham, *ibid.* **140**, A1133 (1965).
- [41] P. Giannozzi, S. Baroni, N. Bonini, M. Calandra, R. Car, C. Cavazzoni, D. Ceresoli, G. L. Chiarotti, M. Cococcioni, I. Dabo, A. Dal Corso, S. de Gironcoli, S. Fabris, G. Fratesi, R. Gebauer, U. Gerstmann, C. Gougoussis, A. Kokalj, M. Lazzeri, L. Martin-Samos, N. Marzari, F. Mauri, R. Mazzarello, S. Paolini, A. Pasquarello, L. Paulatto, C. Sbraccia, S. Scandolo, G. Sclauzero, A. P. Seitsonen, A. Smogunov, P. Umari, and R. M. Wentzcovitch, *J. Phys.: Condens. Matter* **21**, 395502 (2009).
- [42] <https://www.quantum-espresso.org>.
- [43] N. Troullier and J. L. Martins, *Phys. Rev. B* **43**, 1993 (1991).
- [44] H. Fu and O. Gulseren, *Phys. Rev. B* **66**, 214114 (2002).
- [45] E. Sawaguchi, *J. Phys. Soc. Jpn.* **7**, 110 (1952).
- [46] W. Zhong, R. D. King-Smith, and D. Vanderbilt, *Phys. Rev. Lett.* **72**, 3618 (1994).
- [47] R. D. King-Smith and D. Vanderbilt, *Phys. Rev. B* **47**, 1651 (1993).
- [48] R. Resta, *Rev. Mod. Phys.* **66**, 899 (1994).
- [49] A. Raeliarijaona and H. Fu, *Phys. Rev. B* **92**, 094303 (2015).
- [50] A. Filippetti, V. Fiorentini, F. Ricci, P. Delugas, and J. Iniguez, *Nat. Commun.* **7**, 11211 (2016).
- [51] J. T. Last, *Phys. Rev.* **105**, 1740 (1957).
- [52] J. Hlinka, J. Petzelt, S. Kamba, D. Noujni, and T. Ostapchuk, *Phase Trans.* **79**, 41 (2006).
- [53] J. C. Slater, *Phys. Rev.* **78**, 748 (1950).
- [54] M. Fornari and D. J. Singh, *Phys. Rev. B* **63**, 092101 (2001).
- [55] P. M. Gehring, S. E. Park, and G. Shirane, *Phys. Rev. Lett.* **84**, 5216 (2000).
- [56] J. Hlinka, S. Kamba, J. Petzelt, J. Kulda, C. A. Randall, and S. J. Zhang, *Phys. Rev. Lett.* **91**, 107602 (2003).